[redacted]

741

HEAO-1
REDUCED X-RAY COUNT DATA
77-075A-03A

HEAO-1
REDUCED X-RAYSCANNING DATA
77-075A-03B

HEAO-2
X-RAY DATA OF JOVIAN AURORAE
78-103A-02C

HEAO 1

REDUCED X-RAY COUNT DATA

77-075A-03A

This data set has been restored. There were originally three 9-track, 1600 BPI tapes written in Binary. There is one restored tape. The DR tape is a 3480 cartridge and the DS tape is 9-track, 6250 BPI. The original tapes were created on a 3081 computer and the restored tapes were created on an IBM 9021 computer. The DR and DS numbers along with the corresponding D numbers are as follows:

DR#	DS#	D#	FILES
DR004823	DS004823	D043233	1
		D043234	2
		D043235	3

o D043235: Read error occurred in record 4176 of file 1.

77-075A-03A

HEAO-1

REDUCED X-RAY COUNT DATA

THIS DATA SET CONSISTS OF 3 TAPES. THE TAPES ARE 9-TRACK, 1600 BPI, BINARY, WITH 1 FILE OF DATA AND CREATED ON AN IBM 360 COMPUTER. THE DD AND DC NUMBERS ALONG WITH THEIR TIME SPANS ARE AS FOLLOWING:

DD#	DC#	TIME SPANS
D-43233	C-29051	01/06/77-01/20/77
D-43234	C-29052	01/11/77-03/08/77
D-43235	C-29053	02/09/77-02/04/77(?)

HEAO-1
77-075A-03A
REDUCED X-RAY COUNT DATA

All tapes contain 1 file. All records are duplicated. The 1st two records of each tape are an ASCII index of the tapes contents (described on pg.3 of format). Record 2 is a repeat of record 1 to ensure recovery if the 1st record is lost due to a parity error.

The 1st 16-bit word of the remaining records is the type code (FFFD=3; FFFE=-2; FFF3= -13; FFF4=-12). The 2nd 16-bit word is the logical record length (16-bit word).

The 1st part of the 3rd record contains a 17 word tape identification record (type-3 pg 1 of format). This is followed by a 316 word header (pgs 3-4 of format). It contains about 50 words of information with the remaining 266 words padded with zeroes. It's followed by a varriable number of source crossing records of 316 words. (pgs 4-5 of format).

The following are the time spans I found:

D-43233	J.Day 371-385	orbits 60-267
D-43234	J.Day 376-432	orbits 134-999
*D-43235	J.Day 405-400	orbits 586-499(?)

D-43235 seems to have a problem with the time span

DUMP OF TAPE KM2005

D43233 01/00| 77-01/20/77 77-075A-03A

INELT TAPE KM2005 ON FTL
DATA INPUT H9 NF=1 SR=1=1=1 SR=1 LAST 10

FILE 1 / RECORD 1 LENGTH 4818BYTES

(0)	FFEDE312	41445830	31000000	00005046	00040000	00090CA9	0FE51218	12180938	00000100	40020317
(40)	54415045	2E46494C	45202020	20202020	20202020	20202020	20202020	20202020	20300D4E	414D4520
(80)	20202020	20202020	20202020	20202020	20202027	41445830	312E5046	2F4E270D	4E414D45	20202020
(120)	20202020	20202020	20202020	20202020	27413130	30303035	502E4458	2F4E270D	4E414D45	20202020
(160)	20202020	20202020	20202020	20202020	27413230	30303035	502E4458	2F4E270D	4E414D45	20202020
(200)	20202020	20202020	20202020	20202020	27413130	30303036	502E4458	2F4E270D	4E414D45	20202020
(240)	20202020	20202020	20202020	20202020	27413230	30303036	502E4458	2F4E270D	4E414D45	20202020
(280)	20202020	20202020	20202020	20202020	27413130	30303037	502E4458	2F4E270D	4E414D45	20202020
(320)	20202020	20202020	20202020	20202020	27413230	30303037	502E4458	2F4E270D	4E414D45	20202020
(360)	20202020	20202020	20202020	20202020	27413130	30303038	502E4458	2F4E270D	4E414D45	20202020
(400)	20202020	20202020	20202020	20202020	27413230	30303038	502E4458	2F4E270D	4E414D45	20202020
(440)	20202020	20202020	20202020	20202020	27413130	30303435	502E4458	2F4E270D	4E414D45	20202020
(480)	20202020	20202020	20202020	20202020	27413230	30303435	502E4458	2F4E270D	4E414D45	20202020
(520)	20202020	20202020	20202020	20202020	27413130	30313031	502E4458	2F4E270D	4E414D45	20202020
(560)	20202020	20202020	20202020	20202020	27413230	30313031	502E4458	2F4E270D	4E414D45	20202020
(600)	20202020	20202020	20202020	20202020	27413130	30313032	502E4458	2F4E270D	4E414D45	20202020
(640)	20202020	20202020	20202020	20202020	27413230	30313032	502E4458	2F4E270D	4E414D45	20202020
(680)	20202020	20202020	20202020	20202020	27413130	30313033	502E4458	2F4E270D	4E414D45	20202020
(720)	20202020	20202020	20202020	20202020	27413230	30313033	502E4458	2F4E270D	4E414D45	20202020
(760)	20202020	20202020	20202020	20202020	27413130	30333030	502E4458	2F4E270D	4E414D45	20202020
(800)	20202020	20202020	20202020	20202020	27413230	30333030	502E4458	2F4E270D	4E414D45	20202020
(840)	20202020	20202020	20202020	20202020	27413130	30333031	502E4458	2F4E270D	4E414D45	20202020
(880)	20202020	20202020	20202020	20202020	27413230	30333031	502E4458	2F4E270D	4E414D45	20202020
(920)	20202020	20202020	20202020	20202020	27413130	30333032	502E4458	2F4E270D	4E414D45	20202020
(960)	20202020	20202020	20202020	20202020	27413230	30333032	502E4458	2F4E270D	4E414D45	20202020
(1000)	20202020	20202020	20202020	20202020	27413130	30333930	502E4458	2F4E270D	4E414D45	20202020
(1040)	20202020	20202020	20202020	20202020	27413230	30333930	502E4458	2F4E270D	4E414D45	20202020
(1080)	20202020	20202020	20202020	20202020	27413130	30343331	502E4458	2F4E270D	4E414D45	20202020
(1120)	20202020	20202020	20202020	20202020	27413230	30343331	502E4458	2F4E270D	4E414D45	20202020
(1160)	20202020	20202020	20202020	20202020	27413130	30343332	502E4458	2F4E270D	4E414D45	20202020
(1200)	20202020	20202020	20202020	20202020	27413230	30343332	502E4458	2F4E270D	4E414D45	20202020
(1240)	20202020	20202020	20202020	20202020	27413130	30343731	502E4458	2F4E270D	4E414D45	20202020
(1280)	20202020	20202020	20202020	20202020	27413230	30343731	502E4458	2F4E270D	4E414D45	20202020
(1320)	20202020	20202020	20202020	20202020	27413130	30343732	502E4458	2F4E270D	4E414D45	20202020
(1360)	20202020	20202020	20202020	20202020	27413230	30343732	502E4458	2F4E270D	4E414D45	20202020
(1400)	20202020	20202020	20202020	20202020	27413130	31313030	502E4458	2F4E270D	4E414D45	20202020
(1440)	20202020	20202020	20202020	20202020	27413230	31313030	502E4458	2F4E270D	4E414D45	20202020
(1480)	20202020	20202020	20202020	20202020	27413130	31313031	502E4458	2F4E270D	4E414D45	20202020
(1520)	20202020	20202020	20202020	20202020	27413230	31313031	502E4458	2F4E270D	4E414D45	20202020
(1560)	20202020	20202020	20202020	20202020	27413130	31313032	502E4458	2F4E270D	4E414D45	20202020
(1600)	20202020	20202020	20202020	20202020	27413230	31313032	502E4458	2F4E270D	4E414D45	20202020
(1640)	20202020	20202020	20202020	20202020	27413130	31313430	502E4458	2F4E270D	4E414D45	20202020
(1680)	20202020	20202020	20202020	20202020	27413230	31313430	502E4458	2F4E270D	4E414D45	20202020
(1720)	20202020	20202020	20202020	20202020	27413130	31313531	502E4458	2F4E270D	4E414D45	20202020
(1760)	20202020	20202020	20202020	20202020	27413230	31313531	502E4458	2F4E270D	4E414D45	20202020
(1800)	20202020	20202020	20202020	20202020	27413130	31323230	502E4458	2F4E270D	4E414D45	20202020
(1840)	20202020	20202020	20202020	20202020	27413230	31323230	502E4458	2F4E270D	4E414D45	20202020
(1880)	20202020	20202020	20202020	20202020	27413130	31323232	502E4458	2F4E270D	4E414D45	20202020
(1920)	20202020	20202020	20202020	20202020	27413230	31323232	502E4458	2F4E270D	4E414D45	20202020
(1960)	20202020	20202020	20202020	20202020	27413130	31323233	502E4458	2F4E270D	4E414D45	20202020
(2000)	20202020	20202020	20202020	20202020	27413230	31323233	502E4458	2F4E270D	4E414D45	20202020
(2040)	20202020	20202020	20202020	20202020	27413130	31333330	502E4458	2F4E270D	4E414D45	20202020
(2080)	20202020	20202020	20202020	20202020	27413230	31333330	502E4458	2F4E270D	4E414D45	20202020
(2120)	20202020	20202020	20202020	20202020	27413130	31333331	502E4458	2F4E270D	4E414D45	20202020
(2160)	20202020	20202020	20202020	20202020	27413230	31333331	502E4458	2F4E270D	4E414D45	20202020
(2200)	20202020	20202020	20202020	20202020	27413130	31333332	502E4458	2F4E270D	4E414D45	20202020
(2240)	20202020	20202020	20202020	20202020	27413230	31333332	502E4458	2F4E270D	4E414D45	20202020

77-075A-03B

HEAO 1

77-075A-03B

THIS DATA SET CONSISTS OF 100 TAPES. THE TAPES ARE 9-TRACK, 1600 BPI, WITH 1 FILE OF DATA EACH, AND CREATED ON AN IBM 360 COMPUTER THE D AND C NUMBERS ALONG WITH THIER CORRESPONDING TIME SPANS ARE AS FOLLOWING:

D#	C#	TIME SPANS
D-66391	C-28940	
D-66392	C-28941	
D-66393	C-28942	
D-66394	C-28943	
D-66395	C-28944	
D-66396	C-28945	
D-66397	C-28946	
D-66398	C-28947	
D-66399	C-28948	
D-66400	C-28949	
D-66401	C-28950	
D-66402	C-28951	
D-66403	C-28952	
D-66404	C-28953	
D-66405	C-28954	
D-66406	C-28955	
D-66407	C-28956	
D-66408	C-28957	
D-66409	C-28958	
D-66410	C-28959	
D-66411	C-28960	
D-66412	C-28961	
D-66413	C-28962	
D-66414	C-28963	
D-66415	C-28964	
D-66416	C-28965	
D-66417	C-28966	
D-66418	C-28967	
D-66419	C-28968	
D-66420	C-28969	
D-66421	C-28970	
D-66422	C-28971(ordering replacement tape)	
D-66423	C-28972	
D-66424	C-28973	
D-66425	C-28974	
D-66426	C-28975	
D-66427	C-28976	
D-66428	C-28977	
D-66429	C-28978	
D-66430	C-28979	
D-66431	C-28980	
D-66432	C-28981(ordering replacement tape)	

D-66433	C-28982
D-66434	C-28983
D-66435	C-28984
D-66436	C-28985
D-66437	C-28986
D-66438	C-28987
D-66439	C-28988
D-66440	C-28989
D-66441	C-28990
D-66442	C-28991
D-66443	C-28992
D-66444	C-28993
D-66445	C-28994
D-66446	C-28995
D-66447	C-28996
D-66448	C-28997
D-66449	C-28998
D-66450	C-28999
D-66451	C-29000
D-66452	C-29001
D-66453	C-29002
D-66454	C-29003
D-66455	C-29004
D-66456	C-29005
D-66457	C-29006
D-66458	C-29007
D-66459	C-29008
D-66460	C-29009
D-66461	C-29010
D-66462	C-29011
D-66463	C-29012(ordering replacement tape)
D-66464	C-29013
D-66465	C-29014
D-66466	C-29015
D-66467	C-29016
D-66468	C-29017
D-66469	C-29018
D-66470	C-29019
D-66471	C-29020
D-66472	C-29021
D-66473	C-29022(ordering replacement tape)
D-66474	C-29023
D-66475	C-29024
D-66476	C-29025
D-66477	C-29026
D-66478	C-29027
D-66479	C-29028(ordering replacement tape)
D-66480	C-29029
D-66481	C-29030
D-66482	C-29031
D-66483	C-29032
D-66484	C-29033
D-66485	C-29034
D-66486	C-29035
D-66487	C-29036
D-66488	C-29037
D-66489	C-29038
D-66490	C-29089

77-0154-03B

Center for Astrophysics
60 Garden Street
Cambridge, Massachusetts 02138

Harvard College Observatory
Smithsonian Astrophysical Observatory

June 3, 1985

Dr. S.J. Kim
Acquisition Scientist
National Space Science Data Center
Goddard Space Flight Center
Code 633.4
Greenbelt, Maryland 20771

Dear Dr. Kim:

I was happy to receive your letter dated February 25 reopening the contact between our HEAO A-3 group and the NSSDC. We have indeed neglected data submission recently although we have been progressing with what we proposed to NASA as necessary to "preserve the scientific data base," of our experiment. My basic plan now is to proceed with the latter submission. I enclose part I of that NASA proposal, which you should use as a basic reference to our experiment. In reference to the data products listed on page 12, we are mailing by separate cover item 3. This contains 10 boxes, each with 10 magnetic tapes. (This constitutes official return of 100 of the magnetic tapes provided to us by GSFC.) I now propose that the high ecliptic latitude BCAT, and the complete BDCAT -.DX files will complete the A-3 archival reduced data submission. These two items will be prepared and submitted in FY1986, which I understand NASA is planning as the final "phase-down" year for HEAO-1. The corollary software and documentation products discussed in sections 2.3 and 2.4 of our proposal are available, but I would appreciate your thoughts as to their suitability and usefulness to the NSSDC. I enclose with this letter a copy of the format documentation for the -.DX files.

The analyzed flight data to be submitted remains as planned in section 2.2 of our proposal. In this regard we have previously submitted approximately 100 finding charts of sources in 50 publications. I enclose an additional 7 preprints of more recent work. Again, I would appreciate your thoughts on the usefulness of the publication itself, or whether we would do better to extract just the 8 1/2 x 11 glossy finding chart to submit. I will add your name to our mailing list so that you automatically receive future A-3 publications. We plan to submit the material for unidentified sources, discussed on page 17 of the enclosed proposal, in FY86, at the planned conclusion of our current efforts.

Please feel free to contact me for further information on our experiment, or discussion of our reduced and analyzed data products.

Sincerely yours,

Dan Schwartz

Daniel A. Schwartz
Principal Investigator
HEAO-1 A-3

DAS/di
Encl: Proposal P1192-6-82, Part I
Formats, Documentation
Scanning Modulation Collimator Preprints (7).

cc:
H. Bradt
W. Roberts
B. Rowe
H. Tananbaum
L. Kaluzienski

DATE: 1/5/81
AUTHOR: M. CONROY

THE FOLLOWING DOCUMENTATION PERTAINS TO FORMATS FOR MERGED DATA FILES FROM THE HEAO-1 A3 EXPERIMENT AND IS GIVEN IN TWO SECTIONS. THE FIRST PROVIDING INFORMATION ON RETRIEVING DATA FILES FROM MAGNETIC TAPE, AND THE SECOND DETAILING THE ACTUAL DATA RECORDS AS THEY WILL APPEAR ON DISK.

THE MERGED DATA FILES FROM THE HEAO-1 A3 EXPERIMENT ARE DUMPED ON 9-TRACK MAGNETIC TAPE AT 1600 BPI, USING 16 BIT WORDS AND VARIABLE LENGTH RECORDS (A MAXIMUM OF 4095 WORDS). EACH TAPE RECORD WILL BEGIN WITH ONE OF THE FOLLOWING TYPE CODES. THERE ARE 4 POSSIBLE RECORD TYPE CODES DESCRIBED AS FOLLOWS:

TYPE CODE : -3
LEN : 18

WORD 0 - 4	FILENAME
WORD 5	FILENAME 2 CHARACTER EXTENSION
WORD 6	N/A
WORD 7	N/A
WORD 8	BLOCK COUNT OF FILE -1 (USING 256 WORD BLOCKS)
WORD 9	BYTE COUNT IN LAST BLOCK
WORD 10	N/A
WORD 11	YEAR/DAY LAST ACCESSED
WORD 12	YEAR/DAY CREATED OR MOST RECENTLY MODIFIED
WORD 13	HOUR/MIN CREATED OR MOST RECENTLY MODIFIED
WORD 14	N/A
WORD 15	N/A
WORD 16	N/A
WORD 17	N/A
WORD 18	N/A
WORD 19-END	DATA

THIS INDICATES THE START OF A NEW DATA FILE. THE FIRST 18 WORDS IDENTIFIES WHICH DATA FILE AND ARE FOLLOWED IMMEDIATELY BY THE DATA.

TYPE CODE : -13
LEN : 18

THIS INDICATES THAT THIS TAPE RECORD IS AN EXACT DUPLICATE OF THE PREVIOUS TYPE CODE -3 RECORD. THESE ARE FOUND WHEN THE DATA WAS 'DOUBLE-DUMPED' TO ENSURE RECOVERY IF THE FIRST TAPE RECORD CONTAINED A PARITY ERROR. IF NO ERROR OCCURRED ON THE READ OF THE TYPE CODE -3 RECORD, THE TYPE CODE -13 RECORDS SHOULD ALWAYS BE IGNORED.

TYPE CODE : -2
LEN : 0

THIS INDICATES THAT THIS TAPE RECORD IS DATA WHICH BELONGS TO THE FILE DESCRIBED IN THE LAST TYPE CODE -3 RECORD. THE 0 LENGTH MEANS THAT THE RECORD CONTINUES FROM THIS POINT TO THE END OF THIS TAPE RECORD. THE TAPE RECORD WILL BE EITHER 4095 WORDS OR AS MANY WORDS AS NECESSARY

TO COMPLETE THIS DATA FILE, WHICHEVER IS SHORTER.

TYPE CODE : -12
LEN : 0

THIS INDICATES THAT THIS TAPE RECORD IS AN EXACT DUPLICATE OF THE PREVIOUS TYPE CODE -2 RECORD. THESE ARE FOUND WHEN THE DATA WAS 'DOUBLE-DUMPED' TO ENSURE RECOVERY IF THE FIRST TAPE RECORD CONTAINED A PARITY ERROR. IF NO ERROR OCCURRED ON THE READ OF THE TYPE CODE -2 RECORD THE TYPE CODE -12 RECORDS SHOULD ALWAYS BE IGNORED.

AUTHOR: E.J. RALPH
DATE: 12/10/80

THIS SECTION OF THE DOCUMENTATION IS A DESCRIPTION OF THE DATA FILES THEMSELVES. THERE ARE ALWAYS TWO FILES FOR EACH X-RAY SOURCE, ONE FOR DATA FROM EACH OF THE TWO COLLIMATORS. THE FILES THEMSELVES ARE NAMED ACCORDING TO THE FORMAT

A1*****P.DX
A2*****P.DX

WHERE A IS A PREFIX DENOTING WHICH SET OF 1000 ORBITS THE DATA IS FROM, (A = 0-999, B = 1000-1999, ETC.), FOLLOWED BY A 1 OR 2 WHICH SPECIFIES MC1 (30 ARC-SECOND COLLIMATOR) OR MC2 (120 ARC-SECOND COLLIMATOR), ***** IS THE NUMBER OF THE SOURCE IN THE BINNING CATALOG, AND P.DX IS A STANDARD SUFFIX. (A PRINTED COPY OF THE NUMBERS OF THE X-RAY SOURCES IN THE BINNING CATALOG, THEIR NAMES, AND THEIR POSITIONS WILL BE SUBMITTED WITH THE TAPES.)

IN GENERAL, THERE WILL BE ONLY ONE TAPE FILE ON EACH TAPE AND ALL DATA FILES WILL BE FOUND ON TAPE FILE 0. THE FIRST DATA FILE WILL BE AN INDEX OF THE TAPE CONTENTS AND IS NAMED ACCORDING TO THE FORMAT

ADX**.PF

WHERE A IS THE SAME PREFIX AS ABOVE, DX IS STANDARD, AND ** IS THE NUMBER IN THE WHOLE SERIES OF TAPES OF THAT THOUSAND-ORBIT BATCH .

EACH -.DX FILE IS COMPRISED OF ONE 316 WORD HEADER RECORD AND SOME NUMBER (DEPENDING UPON THE NUMBER OF SOURCE CROSSINGS) OF 316 WORD INDIVIDUAL CROSSING RECORDS. THE HEADER RECORD HAS ONLY ABOUT 50 WORDS OF INFORMATION BUT IS PADDED WITH ZEROES TO 316 WORDS FOR CONSISTENCY. THESE RECORDS BREAK DOWN AS FOLLOWS:

DP - DOUBLE PRECISION
I - INTEGER
R - REAL
IA - INTEGER ARRAY
RA - REAL ARRAY

WORD	TYPE	LENGTH	DESCRIPTION
HEADER RECORD--			
1	DP	4	DOUBLE PRECISION TIME (JD)OF MINOR FRAME AT CENTER OF CROSSING
5	3I	3	TIME OF FILE CREATION
8	3I	3	DATE OF FILE CREATION
11	I	1	SOURCE # IN BINNING CATALOG
12	I	1	MC1 OR MC2
13	3RA	18	SOURCE VECTORS
31	IA	10	SOURCE NAME

41	3R	6	TWEAK ANGLES
47	R	2	FULL WIDTH HALF MAXIMUM FOR MC
49	R	2	BAND SPACING

SOURCE CROSSING RECORD--

1	DP	4	DOUBLE PRECISION TIME (JD) OF MINOR FRAME AT CENTER OF CROSSING
5	I	1	MINOR FRAME AT CENTER OF CROSSING
6	I	1	COLLIMATOR #
7	I	1	ORBIT #
8	I	1	SOURCE # IN OUR CATALOG
9	I	1	SUN PRESENCE/ABSENCE
10	I	1	AZIMUTH RESIDUALS FOR ORBIT (ASPECT)
11	I	1	ELEVATION RESIDUALS FOR ORBIT (ASPECT)
12	I	1	# GOOD STARS (ASPECT)
13	I	1	# BAD STARS (ASPECT)
14	I	1	# TOTAL STARS (ASPECT)
15	I	1	AZIMUTH RESIDUALS FOR SEGMENT (ASPECT)
16	I	1	ELEVATION RESIDUALS FOR SEGMENT (ASPECT)
17	R	2	AVERAGE ANGLE TO SOLID EARTH
19	R	2	AVERAGE RATE (SUMMED CHANNELS ABC)
21	R	2	AVERAGE RATE (CHANNEL A)
23	R	2	AVERAGE RATE (CHANNEL B)
25	R	2	AVERAGE RATE (CHANNEL C)
27	R	2	SINGLE BIN MAXIMUM RATE (SUMMED CHANNELS ABC)
29	R	2	SINGLE BIN MAXIMUM RATE (CHANNEL A)
31	R	2	SINGLE BIN MAXIMUM RATE (CHANNEL B)
33	R	2	SINGLE BIN MAXIMUM RATE (CHANNEL C)
35	R	2	SINGLE BIN MINIMUM RATE (SUMMED CHANNELS ABC)
37	R	2	SINGLE BIN MINIMUM RATE (CHANNEL A)
39	R	2	SINGLE BIN MINIMUM RATE (CHANNEL B)
41	R	2	SINGLE BIN MINIMUM RATE (CHANNEL C)

43	R	2	AVERAGE PSD RATE
45	I	1	AVERAGE PSD EXPOSURE
46	R	2	AVERAGE ELEVATION
48	R	2	AVERAGE ELEVATION RESIDUALS (RMS)
50	R	2	AVERAGE AZIMUTH
52	R	2	AVERAGE AZIMUTH RESIDUALS (RMS)
54	R	2	SUMMED TRANSMISSION
56	R	2	SUMMED ELEVATION
58	R	2	SUMMED ELEVATION SQUARED
60	R	2	SUMMED AZIMUTH
62	R	2	SUMMED AZIMUTH SQUARED
64	I	1	SUMMED EXPOSURE
65	R	2	JITTER ANGLE: SUMMED COSINES
67	R	2	SUMMED SINES
69	R	2	SUMMED COS SQUARED
71	R	2	SUMMED SINE SQUARED
73	I	1	AVERAGE Z AXIS RA
74	I	1	AVERAGE Z AXIS DEC
75	I	1	MINOR FRAME OF SUNRISE
76	I	1	NOT USED
77	IA	60	BINNED COUNTS (CHANNEL A)
137	IA	60	BINNED COUNTS (CHANNEL B)
197	IA	60	BINNED COUNTS (CHANNEL C)
257	IA	60	BINNED EXPOSURE

do a hex dump of last 2 tapes of Dataset 1st and last 8 records

p.1

HEAO-1 - (77-075A-03B)

D-66441

DUMP OF TAPE VR02001

INPUT TAPE VR02001 ON HT
DATA INPUT H9 NF=1 SR=1=3=3

FILE 1 RECORD 3 LENGTH 8190BYTES

(0)	FFFD0012	41313133	3034300E	00004458	00040000	013E0200	E0241218	1218E830	00000100	40010217
(40)	431A5B68	123A8030	0016001D	00010009	000307BC	32F00001	C02165CB	BF99399B	40FDA1A2	40469016
(80)	C0F6154F	00000000	40F3CE6F	4045E8F3	4022BE57	33483133	30342E38	36202020	20202000	00000000
(120)	412C28FE	3F2CE690	00000000	3C92EACB	3E495EC9	00000000	00000000	00000000	00000000	00000000
(160)	00000000	00000000	00000000	00000000	00000000	00000000	00000000	00000000	00000000	00000000
(200)	00000000	00000000	00000000	00000000	00000000	00000000	00000000	00000000	00000000	00000000
(240)	00000000	00000000	00000000	00000000	00000000	00000000	00000000	00000000	00000000	00000000
(280)	00000000	00000000	00000000	00000000	00000000	00000000	00000000	00000000	00000000	00000000
(320)	00000000	00000000	00000000	00000000	00000000	00000000	00000000	00000000	00000000	00000000
(360)	00000000	00000000	00000000	00000000	00000000	00000000	00000000	00000000	00000000	00000000
(400)	00000000	00000000	00000000	00000000	00000000	00000000	00000000	00000000	00000000	00000000
(440)	00000000	00000000	00000000	00000000	00000000	00000000	00000000	00000000	00000000	00000000
(480)	00000000	00000000	00000000	00000000	00000000	00000000	00000000	00000000	00000000	00000000
(520)	00000000	00000000	00000000	00000000	00000000	00000000	00000000	00000000	00000000	00000000
(560)	00000000	00000000	00000000	00000000	00000000	00000000	00000000	00000000	00000000	00000000
(600)	00000000	00000000	00000000	00000000	00000000	00000000	00000000	00000000	00000000	00000000
(640)	00000000	00000000	00000000	00000000	00000000	00000000	00000000	00000000	431A5B68	123A8030
(680)	00470001	034232F0	00010000	00080031	00030000	FFFFFFFF	426CEBAD	407D7D7D	40115728	402397F5
(720)	40488E5F	41120000	40666666	40E00000	40CCCCCC	40199999	00000000	00000000	00000000	414C31C7
(760)	0241412D	A2643F83	C1E0BE72	E5FD4112	78094246	D3514364	00DE4411	D42BC6FB	CA00432E	B7DAC231
(800)	4227C18D	4322F88E	412D14B7	4322E25C	8BF8F952	2C520000	00000000	00010000	00000000	00000000
(840)	00010000	00000001	00010000	00000000	00010001	00000001	00000000	00020001	00010000	00000000
(880)	00020000	00000004	00010001	00020000	00000000	00010000	00010001	00020002	00000000	00010001
(920)	00000002	00000003	00010001	00000000	00000001	00000000	00020005	00010002	00010000	00020000
(960)	00000002	00010002	00010003	00030002	00010000	00010001	00020002	00020001	00000001	00010000
(1000)	00000001	00010001	00020004	00020004	00010000	00000001	00030000	00020001	00010001	00000001
(1040)	00000002	00000000	00010000	00010003	00030001	00010001	00020002	00020002	00000002	00030003
(1080)	00010001	00040003	00000005	00020008	00020001	00050004	00030003	00030001	00060001	00050001
(1120)	00020003	00000002	00020004	00030003	00020001	00020002	00030002	00000004	00060003	00020007
(1160)	00010004	00020002	00010004	00030001	00050006	00010001	0009000A	00090008	00080009	00090009
(1200)	0007000A	00080009	00090009	000A000A	000A0009	00090009	000A0009	0008000A	0009000B	0009000A
(1240)	0008000A	000A000A	000A0008	000A000A	000A000A	0008000A	0009000A	000A0008	000A000A	000A000A
(1280)	0008000A	000A000A	000A0009	0009000A	000A000A	00090009	431A5ECC	8E688030	22260001	034232F0
(1320)	FFFF000C	00080031	0003000E	0009000A	42E4D874	41EEEF6E	401FE92D	401EFC4F	404CE9E9	41180000
(1360)	40800000	41100000	41100000	00000000	00000000	00000000	00000000	414DC71C	0240412F	CFEF3F5B
(1400)	3ECEC0CF	984C40AF	46E04227	E73F4340	CED443C1	AC9BC311	96374318	6D98015B	421AAEA9	43159F36
(1440)	4120D432	431EEED8	8C34F980	2C520000	00000000	00000001	00010000	00000002	00010001	00020001
(1480)	00000001	00000000	00020001	00000001	00000002	00000000	00000002	00000001	00020001	00010000
(1520)	00030000	00020001	00000001	00010000	00010000	00000000	00000000	00000000	00010002	00010001
(1560)	00010001	00010000	00000000	00020001	00010003	00000001	00010001	00010000	00020000	00000000
(1600)	00010000	00010000	00010000	00000001	00000000	00010000	00020000	00010000	00020001	00000000
(1640)	00000000	00010001	00000001	00000001	00020000	00000000	00010000	00020002	00020001	00000001
(1680)	00030000	00000000	00000000	00010002	00020001	00000003	00010002	00000005	00030003	00000001
(1720)	00000001	00020003	00040004	00010000	00040001	00010001	00000001	00010003	00020001	00010002
(1760)	00000002	00010001	00020004	00030004	00020005	00000002	00000002	00010001	00000000	00040003
(1800)	00010001	00000001	00030004	00030000	00030007	00070007	00060006	00020007	00070007	00060006
(1840)	00020007	00070007	00060006	00020006	00060006	00050006	00030007	00070006	00070006	00020007
(1880)	00070006	00070006	00020007	00070006	00060006	00030007	00070007	00050007	00020007	00070007
(1920)	00060006	00020007	00070007	00060005	431A61FB	21FFAD52	20A70001	034832F0	FFFF0010	000A0034
(1960)	0002000F	00110008	4257C668	4067E73D	4013E578	401E81FD	40357FC7	40FFFFFF	404CCCCC	40666666

Skip to p. 4

(7280)	00010002	00010005	[illegible]	00000000	00010002	00000003	00000000	00000002	00010000	00010002
(7320)	00010002	00000003	00000003	00000002	00000000	00000004	00010001	00020000	00010002	00000001
(7360)	00030000	00040000	00020000	00010003	00010000	00000001	00000000	00010003	00020002	00030003
(7400)	00000002	00010000	00000005	00020001	00020001	00010003	00020001	00000000	00030001	00020002
(7440)	00020002	00040005	00010000	00030000	00040001	00010007	00030001	00000001	00020003	00060004
(7480)	00010001	00020000	00010002	00030000	00030004	00010000	00070007	00070006	00070008	00070009
(7520)	00080007	00080008	00080008	00070008	00080008	00080008	00080007	00080007	00090007	00070008
(7560)	00080008	00080008	00080008	00080007	00090007	00080008	00080008	00080008	00080008	00070008
(7600)	00080007	00080008	00080008	00080008	00070008	00080007	431A69C3	331F8B87	00180001	035032F0
(7640)	00010000	0000003E	00020000	FFFFFFFF	425EE73E	4079E79E	40138138	401D41D4	40492492	41180000
(7680)	41100000	41100000	41180000	00000000	00000000	00000000	00000000	414E0000	C100412A	3C973F11
(7720)	E377411A	4CC24[illegible]34	E71241BA	17F24311	4DEE432D	A12642AC	97BA4312	02E70069	41A05CC2	4268851C
(7760)	40F4EAA1	42680AF6	8CEFF900	2DF90000	00000000	00000000	00010000	00000000	00000000	00000000
(7800)	00000000	00000001	00000000	00000000	00010000	00000000	00000001	00010000	00000000	00000000
(7840)	00000000	00000000	00000000	00000001	00000000	00000000	00000000	00000000	00000000	00000000
(7880)	00000000	00010001	00000000	00000000	00020000	00000000	00000000	00000000	00010001	00010000
(7920)	00000000	00000000	00000000	00000000	00000000	00000000	00000001	00010000	00000001	00000001
(7960)	00000000	00000000	00000000	00000000	00000000	00000001	00000000	00000000	00000000	00000000
(8000)	00010000	00000000	00000000	00000001	00000001	00000001	00000001	00010000	00000000	00000001
(8040)	00000000	00000000	00000001	00010000	00000000	00000000	00010001	00000001	00010001	00010002
(8080)	00000000	00000003	00000000	00020001	00000000	00010000	00010001	00000000	00000001	00000002
(8120)	00000000	00000002	00000000	00000001	00020002	00020002	00020002	00020002	00020001	00010001
(8160)	00010000	00010001	00010001	00010001	00010002	00020002	00020002	0002		

source # 1304

FILE 1 RECORD 1 LENGTH 8190 BYTES

(0)	FFF30012	41310133	30340050	00004458	00040000	013E0200	E0241218	12180830	00000100	40010217
(40)	431A5B68	123A8030	0016[illegible]1D	00010005	000307EC	32F00001	C021E5CE	EF59595B	40FDA1A2	40465016
(80)	C0F6154F	00000000	40F3CE6F	4045E8F3	4022BE57	33483133	30342B38	36202020	20202000	00000000
(120)	413C2EFE	3F2C6690	00000000	3D92EACB	3E455EC9	00000000	00000000	00000000	00000000	00000000
(160)	00000000	00000000	00000000	00000000	00000000	00000000	00000000	00000000	00000000	00000000
(200)	00000000	00000000	00000000	00000000	00000000	00000000	00000000	00000000	00000000	00000000
(240)	00000000	00000000	00000000	00000000	00000000	00000000	00000000	00000000	00000000	00000000
(280)	00000000	00000000	00000000	00000000	00000000	00000000	00000000	00000000	00000000	00000000
(320)	00000000	00000000	00000000	00000000	00000000	00000000	00000000	00000000	00000000	00000000
(360)	00000000	00000000	00000000	00000000	00000000	00000000	00000000	00000000	00000000	00000000
(400)	00000000	00000000	00000000	00000000	00000000	00000000	00000000	00000000	00000000	00000000
(440)	00000000	00000000	00000000	00000000	00000000	00000000	00000000	00000000	00000000	00000000
(480)	00000000	00000000	00000000	00000000	00000000	00000000	00000000	00000000	00000000	00000000
(520)	00000000	00000000	00000000	00000000	00000000	00000000	00000000	00000000	00000000	00000000
(560)	00000000	00000000	00000000	00000000	00000000	00000000	00000000	00000000	00000000	00000000
(600)	00000000	00000000	00000000	00000000	00000000	00000000	00000000	00000000	00000000	00000000
(640)	00000000	00000000	00000000	00000000	00000000	00000000	00000000	00000000	431A5B68	123A8030
(680)	08470001	034232F0	0001000C	00080031	00030000	FFFFFFFF	426CEEAD	407D7D7D	40115728	402397F5
(720)	4148EE5F	41120000	41666666	40800000	40CCCCCC	40199999	00000000	00000000	00000000	414C31C7
(760)	024[illegible]412D	A2643F83	C1E0BE72	E5FC4112	78054246	C3514364	00DE4411	E42EC0FE	CA0C432E	B7CA0231
(800)	4227C18D	4322F88E	412D14B7	4322E25C	8BF8F952	2C520000	00000000	00010000	00000000	00000000
(840)	00010000	00000001	00010000	00000000	00010001	00000001	00000000	00020001	00010000	00000000
(880)	00020000	00000004	00010001	00020000	00000000	00010000	00010001	00020002	00000000	00010001
(920)	00000002	00000003	00010001	00000000	00000001	00000000	00020005	00010002	00010000	00020000
(960)	00000002	00010002	00010003	00030002	00010000	00010001	00020002	00020001	00000001	00010000
(1000)	00000001	00010001	00020004	00020004	00010000	00000001	00030000	00020001	00010001	00000001
(1040)	00000002	00000000	00010000	00010003	00030001	00010001	00020002	00020002	00000002	00030003
(1080)	00010001	00040003	00000005	00020008	00020001	00050004	00030003	00030001	00060001	00050001
(1120)	00020003	00000002	00020004	00030003	00020001	00020002	00030002	00000004	00060003	00020007
(1160)	00010004	00020002	00010004	00030001	00050006	00010001	0009000A	00090008	00080009	00090009
(1200)	0007000A	00080009	00090009	000A000A	000A0009	00090009	000A0009	0008000A	0009000E	0009000A
(1240)	0008000A	000A000A	000A0008	000A000A	000A000A	0008000A	0009000A	000A0008	000A000A	000A000A
(1280)	0008000A	000A000A	000A0009	0009000A	000A000A	00090009	431A5ECC	8E8E8830	2226C001	034232F0
(1320)	FFFF0000	00080031	0003000E	0019000A	4254D874	40EEEFEE	401FE52D	401EFC4F	404CE9E9	41180000
(1360)	41800000	41100000	41100000	00000000	00000008	00000000	00000000	414DC71C	0240412F	CFEF3F5B
(1400)	3ECBC0CF	984C40AF	46E04227	B73F4340	CEDA43C1	AC9BC311	96374318	6D98015B	421AAEA9	43159F36
(1440)	4120D432	43158EC8	8C34F980	2C520000	00000000	00000001	00010000	00000002	00010001	00020001
(1480)	00000001	00000000	00020001	00000001	00000002	00000000	00000002	00000001	00020001	00010000
(1520)	00030000	00020001	00000001	00010000	00010000	00000000	00000000	00000000	00010002	00010001
(1560)	00010001	00010000	00000000	00020001	00010003	00000001	00010001	00010000	00020000	00000000
(1600)	00010000	00010000	00010000	00000001	00000000	00010000	00020000	00010000	00020001	00000000

Double Precision JD

end of header

end of data header

DP JD

p. 4

78-103A-02C

78-103A-02C

HEAO-2

X-RAY DATA OF JOVIAN AURORAE

THIS DATA SET CONSISTS OF 1 TAPE. THE TAPE IS 9-TRACK, 1600 BPI, BINARY, WITH 1 FILE OF DATA. IT WAS CREATED ON AN IBM 360 COMPUTER. THE DD AND DC NUMBER ALONG WITH IT'S TIME SPAN IS AS FOLLOWING:

DD#	DC#	TIME SPAN (OBSERVATIONS)
D-73981	C-031237	04/13/79 - 04/13/79
		11/24/79 - 11/24/79
		12/03/79 - 12/03/79

January 27, 1986

Dr. Sang Kim
NSSDC
GSFC/NASA Code 663
Greenbelt, MD 20771

Dear Dr. Kim,

Thank you for your request for Einstein data on Jupiter. The data on Jupiter is contained in the HRI sequence 9999. We have written the original field (.DAT) and three Gaussian smoothings of width 64, 128, and 256 arcsec on the enclosed FITS tape. The tape was made at 1600 bpi. All of the arrays are integer, and have been scaled to a maximum pixel value of 4000. Each field is 256*256 in pixel dimensions, has a resolution of 1 arcsec/ pixel, and was centered on RA 12 36 41, DEC -2 30 35 (pixel values 2150, 2020). Please let us know if you have any difficulties with the enclosed data, or if you require more information.

Sincerely,

Fred Seward

Fred Seward/Sherene Aram

JOURNAL OF GEOPHYSICAL RESEARCH, VOL. 88, NO. A10, PAGES 7731-7741, OCTOBER 1, 1983

THE DETECTION OF X RAYS FROM JUPITER

Albert E. Metzger[1], David A. Gilman[1,2], Joe L. Luthey[1], Kevin C. Hurley[3]
Herbert W. Schnopper[4], Frederick D. Seward[5], James D. Sullivan[6]

Abstract. X rays in the energy band 0.2-3.0 keV have been detected coming from both polar regions of Jupiter. The observations were made in 1979 and 1981 by using the imaging proportional counter and high resolution imaging detectors on the Einstein X ray astronomy satellite. The measured flux density of $\sim 6 \times 10^{-4}$ cm^{-2}s^{-1} at earth corresponds to an X ray luminosity of $\sim 4 \times 10^{9}$ W in the 0.2- to 3.0-keV energy band. The energy spectrum of the X rays is extremely soft and can be characterized by a power law with an exponent of ~ 2.3. Detector energy resolution is insufficient to distinguish a soft line spectrum from a continuum. However, the shape of the response and the observed X ray power indicate that the source of this auroral emission is not electron bremsstrahlung as on the earth, but is most probably line emission from O and S ions with energies between 0.03 and 4.0 MeV/nucleon precipitating from the outer boundary of the Io plasma torus at L $\sim$ 8.

1. Introduction

X rays are generated by the interaction of an energetic particle flux with matter and are produced on a planetary scale in the earth's aurorae [cf. Jones, 1974]. After the existence of the Jovian magnetosphere was established by the observation of nonthermal radio emission [cf. Berge and Gulkis, 1976], estimates of its expected X ray luminosity were made by scaling from terrestrial aurorae to the Jovian field [Hurley, 1972; Heaps et al., 1973]. There was also speculation that bombardment of the Galilean satellites by particle fluxes within Jupiter's magnetosphere would produce substantial characteristic X ray line emission [Mihalov, 1973]. Such a flux could be used to determine surface composition. The search for X ray emission from Jupiter has been conducted since 1964 by balloon [Edwards and McCracken, 1967; Haymes et al., 1968; Hurley, 1972; Mahoney, 1973], rocket [Fisher et al., 1964; Margon, unpublished data, 1969], satellite [Vesecky et al., 1975; Hurley, 1975], and spacecraft [Kirsch et al., 1981]. In this paper we report the first detection of the Jovian X ray flux, an observation made by the Einstein (HEAO-2) Observatory in April 1979 [Metzger et al., 1980], and three subsequent observations that have also yielded positive results.

Because of measurements made by the Pioneer 10 and 11 and the Voyager 1 and 2 spacecraft, [Opp, 1974, 1975; Stone, 1981], we now know that Jupiter's magnetosphere is significantly different from the earth's. On earth, X rays are produced by the same energetic particles that make the visible aurora--trapped and almost trapped electrons supplied by the solar wind and energized by magnetospheric convection-- which precipitate into the atmosphere along high latitude field lines [Jones, 1974; Seltzer and Burger, 1974; Mizera et al., 1978]. Unlike the earth, particles are injected into the Jovian magnetosphere from Io, located deep in the magnetosphere, by means of eruptive gas plumes, atmospheric loss, and surface sputtering [cf. Cheng, 1980; Goertz, 1980a]. These particle fluxes become ionized to form a plasma torus in the neighborhood of Io's orbit [Broadfoot et al., 1979]. Ionization pickup from Jupiter's atmosphere, sputtering from the surfaces of the other Galilean satellites and ring particles, and the solar wind are secondary contributors. The Pioneer and Voyager spacecraft have measured the charged particle and magnetic content of the magnetosphere, but the X ray observations tell something else--the power flowing through the Jovian magnetosphere and the mechanism of energy transfer. We have used the observed X ray spectrum and its spatial distribution to infer the nature of the flux precipitating onto the planet and the power lost from the magnetosphere to the atmosphere in the process. This power is a lower limit to the power delivered to the magnetosphere from the rotation of the planet, the injection of material from orbiting bodies, and the solar wind.

2. Location

2.1. Imaging Proportional Counter Observations

The Einstein Observatory carried an X ray telescope substantially more sensitive than any 2-50 Å (0.2-5 keV) instrument previously placed in orbit [Giacconi et al., 1979]. Of the four detector systems capable of being placed at the focus of the telescope, the position-sensitive imaging proportional counter (IPC) was chosen for the initial observation since it offered the most sensitivity for detection together with good spatial resolution [Gorenstein et al., 1981]. The field of view of the IPC was one square degree, and its effective area averaged 60 cm^2 over an energy range of 0.2 to 4 keV. Its angular resolution was 1 arc min above 1 keV, degrading somewhat with decreasing energy.

[1]Jet Propulsion Laboratory, California Institute of Technology.
[2]now at NASA Headquarters.
[3]Centre d'Etude Spatiale des Rayonnements, CNRS-UPS
[4]Danish Space Research Institute.
[5]Smithsonian Astrophysical Observatory.
[6]Plasma Fusion Center, Massachusetts Institute of Technology.

Paper number 3A1049.
0148-0227/83/003A-1049$05.00

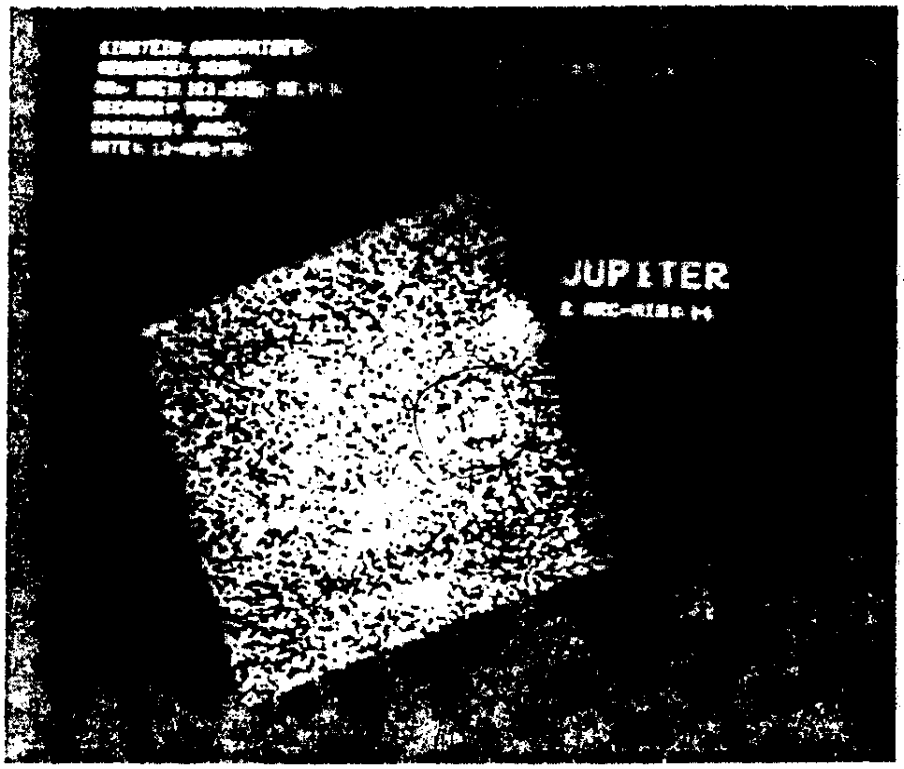

Plate 1. The first X ray image of a planetary body: Jupiter (circle) as seen by the Einstein Observatory satellite on April 13, 1979.

The IPC observations were performed with Jupiter near quadrature in order to satisfy observatory sun-angle constraints and reduce the planet's apparent motion. A probable positive result was obtained on April 13, 1979, but because the source was weak and the field of view rich with sources of comparable intensity, further observations were made on November 24 and December 3, 1979. These confirmed the initial detection, permitted an investigation into the variability of the source, and allowed us to distinguish in part between planetary emission versus possible emission from one or more of the Galilean satellites. Contrasting configurations of Io, Europa, and Ganymede were chosen for the three IPC observations with respect to maximizing their elongation from Jupiter, the possibility of a Jupiter occultation during an observation, and their location east or west of the planet. The observing periods were between 10 and 20 hours long for each of the three observations. During this time, Jupiter moved 1 to 2 arc min across the sky--about the size of the IPC image resolution.

X rays from Jupiter were detected over a range from 0.2 to 3 keV. Plate 1 shows the image obtained in April, 1979. (Note: Plate 1 is shown here in black and white; the color version can be found in the special color section of the journal.) The observing periods, counting rates, and accumulation times for the three IPC observations are shown in Table 1. The background rates were about 30%, 50%, and 70% of the observed counting rates in April, November, and December, respectively, owing to changes in apparent sky brightness. While the November and December observations were made with Jupiter at the center of the field of view, it can be seen from Plate 1 that the telescope nearly missed the planet in the April observation, and a substantial correction for vignetting has been applied to this measurement. The corrected net count rates of the source for the three observations are the same within the experimental uncertainties. More precise values are expected when reprocessed data becomes available.

For each observation, Table 2 shows the separation between the observed source position and the positions of Jupiter and the Galilean satellites. Because the center of the field of view during the April observation was far from the planet, the uncertainty in the position of the source is about 1.0 arc min rather than the 0.7 arc min accuracy obtained for the November and December observations. These uncertainties reflect the overall spectral shape, which is predominantly soft. The expected uncertainty of the three observations combined is 0.99 arc min, so that the RMS combined separation in the last column of Table 2 is also the number of standard deviations.

It can be seen from Table 2 that Jupiter falls closest to the source location when the three observations are considered as a set and that none of the individual separations is large enough to preclude the association. Io is virtually ruled out on the basis of the December observation. Ganymede appears to be eliminated by the November observation, Europa by those of November and December, while Callisto was never a serious possibility, located as it is in the outer part of the magnetosphere. There are additional reasons for ruling out Europa. Europa was east of Jupiter in April and west in November so that its trailing face was visible in April but not in November. Because the Jovian magnetosphere rotates faster than Europa orbits Jupiter, and the particle bounce time is

TABLE 1. Net Source Rates: 0.2-3.0 kev (c/s)

	Time UT Start	Stop	Effective Time, s	Source and Background	Background	Net
April 13, 1979	0100	0639	5986	0.018 ± 0.002	0.006 ± 0.001	0.012 ± 0.002
Nov. 24, 1979	0222	1710	5276	0.025 ± 0.002	0.012 ± 0.001	0.013 ± 0.002
Dec. 2, 1979	0213	0749	8338	0.041 ± 0.002	0.029 ± 0.001	0.012 ± 0.002

short in comparison with the time it takes a field line to pass the satellite, we expect that the trailing face will produce many more X rays than the leading face. No such contrast was observed between the two observations. In addition, Europa was occulted by the planet for 3.2 hours during the April observation without producing a noticeable reduction in the count rate. Io was occulted during portions of both the November and December observations, but unfortunately no useful data was received during these periods.

As Table 1 indicates, the average counting rate is quite constant for the three observations, with a time-weighted average value of 0.012 ±0.002 counts per second from 0.2 to 3.0 keV. We have examined the time profile of each observation with selected time intervals from 500 s to 3000 s. With the exception of one 1000-s period during the December observation, reserved for further study with reprocessed data, no significant (>3σ) flux variation has been seen.

2.2. High Resolution Imager Observation

To confirm that Jupiter is the source of this X ray flux and to determine its distribution at the planet, a fourth observation was scheduled, this time utilizing the high resolution imager (HRI) as the detector [Giacconi et al., 1979]. The HRI consisted of two microchannel plates operated in cascade, followed by a crossed-grid charge detector made of two orthogonal planes of wires. Its field of view was the central 25 arc min of the telescope field, and its angular resolution for a strong source was about 4 arc sec. While responding to essentially the same energy range of 0.15-3 keV as the IPC, the HRI possessed no effective energy resolution.

The HRI observation was performed in January 1981, shortly before the end of the Einstein Observatory's useful lifetime. For this reason less time was available than was considered necessary to assure a positive result, particularly if the source was widely distributed, e.g., as diffuse emission across the planet. Six hours of observation yielded 7336 s of useful data. Despite this limitation, two distinct sources of emission were resolved! The one other source in the field of view was well removed from the Jovian system and not associated with planetary emission.

The two sources at the center of the field of view are shown in Figure 1, superimposed on a map of Jupiter and the Galilean satellites which shows the movement of these objects during the observation. The positions of the two sources are clearly not associated with any of the Galilean satellites. Neither can they be associated with Jupiter's rings which are situated at equatorial latitudes. Both sources clearly represent high latitude near-polar emission from the planet itself.

Plate 2 shows the shape and extent of the two sources as distributions generated by a standard processing routine and smoothed by a Gaussian function. (Note: Plate 2 is shown here in black and white; the color version can be found in the special section of the journal.) The distributions, which present three levels covering a factor of 2 in intensity, are superimposed on a disc of Jupiter placed at its mean position during the observation. The two sources are irregular in shape, with a mean extent of about 20 arc sec. Their maxima lie within 10 arc sec of Jupiter's northern and southern poles. The north-south elongation of

TABLE 2. IPC Observations - Proximity of Source to Mean Position of Jupiter and the Galilean Satellites (arc min)

Object	April 13, 1979	November 24, 1979	December 3, 1979	RMS Combined
Jupiter	0.4	1.6	0.9	1.3
Io	1.9 (W)	0.9 (W)	2.0 (W)	2.1
Europa	0.5 (O-E)	3.9 (E)	3.3 (W)	3.6
Ganymede	1.9 (E)	2.7 (W)	0.4 (E)	2.3
Callisto	5.3 (E)	6.4 (W)	7.8 (E)	8.1

(W), (E), (O) = West, East, Occulted

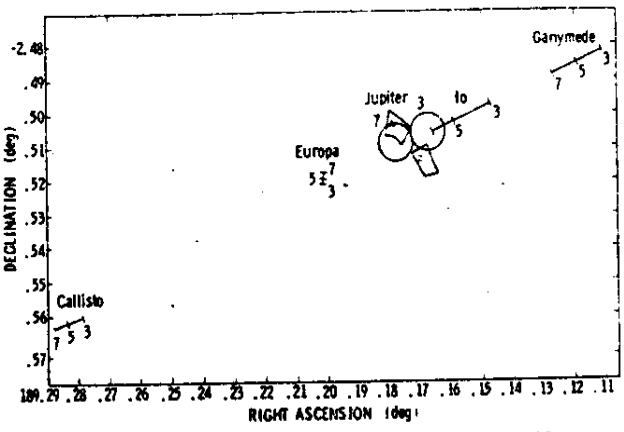

Fig. 1. Location of Jupiter and the Galilean satellites during the high-resolution imaging observation on January 6, 1981. The numbers correspond to position during the observation which began at 2.1 h UT and ended at 7.8 h UT. The quadrilaterals mark the general outline of the two sources associated with Jupiter, the interior squares the approximate location of their maxima.

both sources is greater than expected from instrumental dispersion, which indicates that these are not point sources. The maximum of the southern source is located about 10 arc sec beyond the disc, which indicates the magnitude of the positional error since the atmospheric interaction that generates the X ray flux must occur at scale heights of roughly 1,000 km (~0.5 arc sec) or less. An elongated distribution in the direction of Jupiter's motion is not apparent, suggesting that the source area will broaden when the effect of Jupiter's motion is removed.

The lack of any enhancement in emission a equatorial latitudes shows that no diffuse co ponent has been detected. The relatively sho duration of the observation limits the signif cance of this result.

The measured emission intensities of t northern and southern sources are 3.4 ± 1.1 10^{-3} c/s from the northern source and 3.3 ± 0 x 10^{-3} c/s from the southern, based on 37 and total counts, respectively. The backgroun computed from large source-free areas, amoun to about one-half of this. These rates inclu small corrections for dead time, vignetting, a detector quantum efficiency, and are consiste with the intensities observed in the IPC obse vations, based on the relative efficiencies the two detectors. The combined rate for t two sources corresponds to a luminosity Jupiter of 4 x 10^{16} erg/s.

3. Spectrum

3.1 Observations

In each of the three IPC observati periods the shape of the source spectrum is di tinctly different from the background measu in the immediate vicinity of the source. The (background-subtracted) count rate spectra shown in Figure 2. Associated 1σ uncertaint are based on counting statistics. The upper channels have been paired to improve statisti

The IPC provides only modest spectral re lution, and absorption in the thin polypropyl window results in large variations in the eff tive detector area over the energy range [Gor stein et al., 1981]. To deal with this, HEAO-2 consortium has developed computer co

Plate 2. Intensity distribution of Jupiter's auroral X ray sources superimposed on an outline of the planetary disc. The measurement was made by the High Resolution Imager on the Einstein Observatory. The straight line corresponds to the equator. Motion of the planet is from right to left.

that generate the pulse-height spectrum expected for a model-dependent incident photon spectrum. Within the limitations of detector resolution and low counting rates, we have used these not only to define the range of spectral parameters permitted by the observations, but also to transform net count rates into flux and obtain a representation of the incident spectrum. The best fit parameters obtained by modeling each IPC count rate spectrum for the power law response resulting from electron bremsstrahlung are given in Table 3. The percentile of the χ^2 distribution, F (χ^2), is included to show the quality of fit.

Assuming the incident flux to be a power law and correcting for the instrument response of the detector, the resultant photon flux is shown in Figure 3 and compared with the upper limits established by previous searches. It can be seen that the most sensitive of these fell short of detection by well over an order of magnitude.

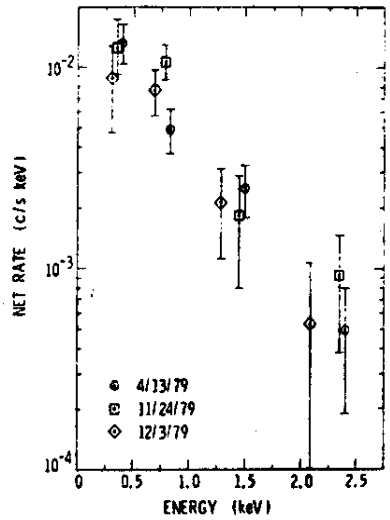

Fig. 2. The X ray count rate spectra from Jupiter for the three imaging proportional counter observations. Channels 3 through 8 have been paired.

3.2. Electron Incidence

Since the observed X rays come from the planet and not from the moons or rings, we can make an estimate of the power delivered to the atmosphere of Jupiter based on the assumption that the incident particles are energetic electrons. Other mechanisms of energy loss exist so this power is a lower limit to the rate at which energy flows through the Jovian magnetosphere.

The efficiency for making X rays as electron bremsstrahlung from hydrogen has been calculated for power law distributions of electrons into hydrogen. These calculations have been made from photon attenuation data tabulated by Veigele [1973], and from extrapolations of cross section tables [Pratt et al., 1977] and electron range tables [Pages et al., 1972]. The effect of scattering on the depth distribution has been neglected in the calculations, but estimates of the scattering give values less than 10^0 for all electrons of interest--hydrogen is not an effective scattering medium. Furthermore, electrons have ranges very much shorter than the mean free paths of equal-energy photons. This means that for electron spectra steeper than E^{-2}, scattering has no effect on the emission efficiency.

The procedure followed was to take an initial power law spectrum of electrons, find the spectrum of electrons at a number of depths in the atmosphere, compute the source function for a given photon energy, and then find the flux of X rays that escape. This was done for ten photon energies between 0.1 and 10 keV, emphasizing the low energy end. The efficiency was computed to be the ratio of emitted X ray luminosity to incoming electron power over the energy range 0.3 to 2.0 keV. Power law spectra were assumed in order to simplify the calculations. This is not a limitation since we find the efficiency over less than a single decade in energy, and over this range almost any continuous spectrum can be approximated by a power law.

For a given photon power law spectral index and intensity, we can then calculate the power in electrons reaching the planet with an uncertainty estimated to be as large as a factor of 3. Figure 4 shows the 90% confidence contours for power law spectral parameters allowed by the three observations, together with the lines corresponding to a range of electron power between 10^{13} and 10^{16} W. The contours fall within a single decade of electron power, from $\sim 10^{15}$ to $\sim 10^{16}$ W. These high levels impose a severe constraint on the energy balance of the magnetosphere which will be discussed in the following section.

3.3. Heavy Ion Incidence

An alternative possibility is that the incident flux consists, not of electrons, but of heavy ions originating in the Io torus [Metzger et al., 1981; Thorne, 1981]. In this case, interactions with atmospheric atoms will result in characteristic line emission with a virtual

TABLE 3. Best Fit Power Law Spectra (0.3 - 3.0 keV)

Observations	Index	Flux erg/cm^{2}s	F(χ^2)
April 13, 1979	2.3	2.7×10^{-3}	0.12
Nov. 24, 1979	2.4	2.0×10^{-13}	0.6
Dec. 3, 1979	2.1	1.5×10^{-13}	0.6

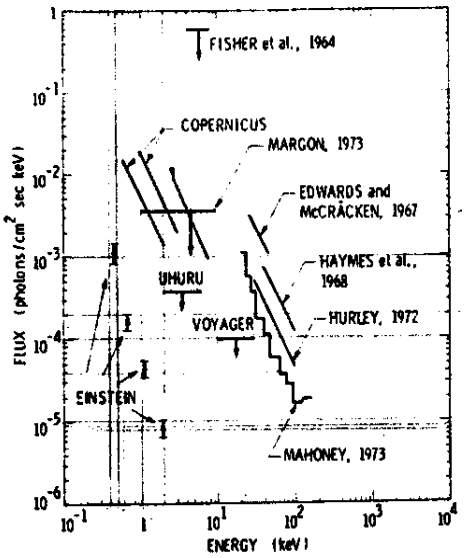

Fig. 3. A comparison of measured upper limits on X ray emission from Jupiter and the initial observation by the Einstein Observatory. Voyager data is by Kirsch et al. [1981], Copernicus data is by Vesecky et al. [1975], Uhuru data by Hurley [1975], and all other data has been compiled by Mahoney [1973].

absence of continuum. The ion-atom collision mechanism is believed to be primarily Coulomb ionization when the ion projectiles are not fully stripped, although electron transfer to bound states of the ions may also contribute [Garcia et al., 1973; Winters et al., 1975]. The major heavy ion constituents near the Io torus as determined by the Voyager ultraviolet spectrometer and plasma science experiments [Bridge et al., 1979; Sandel et al., 1979; Baganel and Sullivan, 1981] are sulfur and oxygen. Modeled as monochromatic K shell line emission spectra, the IPC data produces the fits listed in Table 4. Because the computer program fits one line at a time, the analysis was done separately for the K shell X rays of oxygen at 0.52 keV using a range of 0.25-1.45 keV, and of sulfur at 2.3 keV using a range of 1.45-3.9 keV. Alternative fits over the entire spectrum give an unacceptably high value of χ^2 for sulfur, whereas for the oxygen K line, the fits are about as good as for the power law for two of the three IPC measurements. Although the shape of the incident photon spectra for these two mechanisms of X ray production must contrast sharply, the ability to distinguish between them by means of the observed spectra depends on counting statistics and detector resolution. Both are limited in this case; the integral source strength amounts to 5-6 σ for each observation (Table 1), while the energy resolution (FWHM) of the IPC ranges from 40% at 3 keV to 80% at 0.2 keV. However, the results of the spectral analysis as summarized in Tables 3 and 4 do permit us to conclude that while we cannot discard electron bremsstrahlung based on this data analysis, line emission provides at least as good a fit to the results.

The model-dependent X ray power levels at Jupiter that correspond to the best fit spectra are tabulated in Table 5. Quoted uncertainties incorporate both count rate statistics and possible systematic uncertainties in IPC gain levels, which can fluctuate with time. The three measurements are reasonably consistent for each model; it is possible that the lower power outputs of the December 3, 1979 observation, whether modeled as bremsstrahlung or O_K emission, may be due to overconfining the source area, as the IPC image size spreads substantially at energies below 1 keV. Note that the observed S_K line emission is significantly less intense than the O_K line emission.

4. Discussion

4.1. Source of Power for X rays

Four possible sources of power may be considered responsible for generating Jupiter's X ray flux, i.e., the solar wind, the solar X ray flux, the injection of local material, and planetary rotation. The latter two are internal to the magnetosphere, whereas the solar wind and solar X ray flux provide external energy. The solar wind may be ruled out, as it has been for the UV aurora, since it makes only a minor (~1%) contribution to the total power available within the magnetosphere [Eviatar and Siscoe, 1980].

The possibility that the observed X ray emissions are reflected or secondary solar X rays was considered prior to the HRI observation. Because of the low efficiency of secondary X ray production, the emission induced by the quiet time solar X ray flux fails to account for the observation by a factor of 10^4. This is consistent with observations of X ray emission from the moon in lunar orbit [Adler et al., 1972] and from the sunlit atmosphere of the earth [Rugge, 1978]. And independently, the

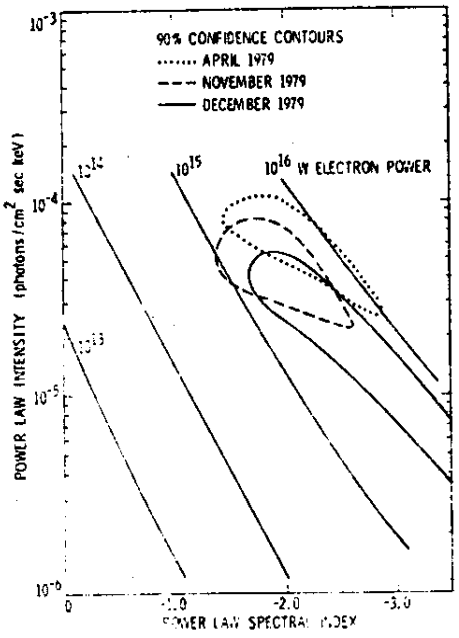

Fig. 4. Ninety percent confidence contours for the power law spectral parameters of the X ray emission, upon which are superimposed the levels of electron power required to generate the X ray flux by electron bremsstrahlung.

TABLE 4. Best Fit Monochromatic Line Spectra

Observation	O_K Line, 0.52 keV		S_K Line, 2.3 keV	
	Flux, erg/cm^{2}s	$F(\chi^2)$	Flux, erg/cm^{2}s	$F(\chi^2)$
April 13, 1979	7.9×10^{-13}	0.8	1.14×10^{-13}	0.3
Nov. 24, 1979	7.4×10^{-13}	0.3	4.5×10^{-14}	0.5
Dec. 3, 1979	4.3×10^{-13}	0.3	7.8×10^{-14}	0.8

fact that X rays are seen only near the poles and not from the equator shows that the X rays are the result of magnetically governed processes and not due to solar X rays.

Within the magnetosphere the amount of material ejected from Io by volcanic emission as a result of gravitational interaction with Jupiter and Europa is substantial [Peale et al., 1979; Cheng, 1980], but it is only weakly energized prior to ionization and acceleration. Furthermore, the degree of ionization is low and the energy provided by corotation is less than 1 keV for both electrons and ions [Bridge et al., 1979], thereby precluding the formation of keV X rays.

It may thus be concluded that Jupiter's X ray emission is powered by the planet's rotation acting through other magnetospheric processes. In fact, the observation of MeV per nucleon ions throughout the middle magnetosphere [Krimigis et al., 1979; Gehrels et al., 1981] demonstrates that the torus is not the only agent for transferring rotational energy to the magnetosphere and also provides a source of flux energetically capable of generating the observed X ray emission. Details of the energizing process and the specific roles played by ions, electrons, and neutral particles is the subject of much current study [cf. Eviatar and Siscoe, 1980; Dessler, 1980; Borovsky et al., 1981; Brown, 1981; Shemansky and Sandel, 1982; Thorne, 1982].

4.2. Sources of Auroral Excitation

Following earlier indications from rocket flights [Giles et al., 1976], the first direct observation of auroral emission at Jupiter was made by the extreme ultraviolet spectrometer on Voyager 1, which also established a relationship between the Io plasma torus and the flux precipitating into Jupiter's atmosphere [Broadfoot et al., 1979; Sandel et al., 1979]. Extreme ultraviolet (EUV) emission does not uniquely identify the nature of the precipitating particles. Electrons, protons, and heavy ions are abundantly present in the plasma torus [Bridge et al., 1979; Broadfoot et al., 1981] and each has been considered as the auroral source.

Although hydrogen constitutes only a minor component within the plasma torus [Shemansky, 1980; Bagenal and Sullivan, 1981], energetic protons have been proposed as the auroral source [Goertz, 1980b]. Protons can generate the observed EUV emission with less power than electrons, and protons are seen to be depleted along field lines that pass through the inner portions of the plasma torus [Krimigis et al., 1979]. However, as Goertz [1980b] has pointed out, X ray emission will not take place from a proton-induced aurora.

4.3. Electrons as the Auroral Source

Auroral emission has most commonly been interpreted as due to electrons precipitating into Jupiter's atmosphere [Broadfoot et al., 1979; Thorne and Tsurutani, 1979; Coroniti et al., 1980; Durrance et al., 1982]. The mechanism considered for precipitation has been the change in pitch angle of electrons scattered by wave-particle interactions [Thorne and Tsurutani, 1979; Thorne, 1981]. Furthermore, Yung et al. [1982] have obtained a discharge spectrum of H_2 by electron impact that closely duplicates spectra of the aurora taken by the IUE spacecraft [Durrance et al., 1982].

The UV aurora is localized close to both polar limbs. Close concordance between the area of the aurora and the projection of magnetic field lines passing through the torus onto the planet has suggested a role for Io's torus as well as for the magnetosphere in delivering plasma to the planet [Broadfoot et al., 1979, 1981; Durrance et al., 1982]. Relative to the mean position of Jupiter, the X ray maxima of the HRI observation are located less than 3 and 10 arc sec from the northern and southern polar limbs respectively, indicating that the X ray

TABLE 5. X Ray Power Levels at Jupiter - IPC Observations
(Based on Spectral Fit to Power Law or Monochromatic Line, 10^9W)

Observation	April 13, 1979	November 24, 1979	December 3, 1983
Bremsstrahlung	2.0 ± 0.4	1.7 ± 0.3	1.2 ± 0.3
O K_α Line Emission (0.52 keV)	5.7 ± 0.9	6.0 ± 0.6	3.3 ± 0.8
S K_α Line Emission (2.3 keV)	0.8 ± 0.3	0.4 ± 0.2	0.6 ± 0.2

production is probably also occurring at the intersection of the field lines from the torus and Jupiter's atmosphere. This implies that X ray and UV emission result from the same basic mechanism.

For the electron-powered aurora, the Voyager EUV team has reported a radiated power level of 5×10^{12} W [Sandel et al., 1979], and from this an input level of 1.2×10^{13} W carried by the precipitating flux [Broadfoot et al., 1981]. This is significantly less than the mean value of 10^{15} W we derive for electron power based on the X ray emission. However, from a revised estimate of the UV excitation efficiency and associated uncertainties, and the probable effect of atmospheric extinction (absorption) on the UV emission, Thorne [1982] calculates an input power range of $0.3\text{-}1.2 \times 10^{14}$ W with a nominal level of more than 6×10^{13} W, given an average energy of 10 keV for the precipitating electrons.

The issue of atmospheric absorption of the auroral flux seems central to the question of whether a real disparity exists between the UV and X ray observations in terms of an electron-powered aurora. The greater the incident electron energy, the deeper its atmospheric penetration and the greater the UV extinction factor. The suggestion that the incident electron flux may be largely confined to 1-30keV [Yung et al., 1982] or limited to lower energies is not supported by the X ray spectrum, which suggests an incident electron distribution extending up to approximately 10 keV. By comparing two wavelength ratios of the Jovian and laboratory discharge spectra [Yung et al., 1982] with a model of the atmosphere [Atreya et al., 1981], Durrance et al. [1982] have deduced that the UV emission takes place at or above an altitude of 330 km, relative to the NH_3 cloud tops at 600 mb. This atmospheric depth corresponds to the range of a 25-keV electron, approximately 10^{-3} g/cm^2. The mean free path of a 0.2-keV X ray has a comparable value so the correction for atmospheric extinction which has been applied already to our bremsstrahlung power calculation is small.

Central to the acceptance of an electron-driven mechanism is whether enough magnetospheric power is contained in an electron-precipitating flux to drive either X ray or UV auroral emission. In order to power the aurora even at the relatively modest level of 1.2×10^{13} W with electrons originating in the torus, the plasma residence time must be less than that required to reach thermal equilibrium [Eviatar and Siscoe, 1980]. However, there is substantial, though not unequivocal, evidence for equilibration. Thermal equilibration corresponds to a mass loading rate in the torus of about 6×10^{27} ions/s [Shemansky, 1980]. An aurora powered by electrons at the level of 1.2×10^{13} W requires a mass loading rate greater than 2×10^{29} ions/s and proportionately more for higher power.

A disparity also exists between the required auroral power and the power deliverable by electrons if the electrons diffuse into the torus after undergoing acceleration in the magnetosphere. The low energy charged particle (LECP) experiment observed large fluxes of energetic electrons in the torus down to its threshold of sensitivity at 30 keV [Armstrong et al., 1981]. These fluxes are depleted in the inner torus [Lanzerotti et al., 1981; Armstrong et al., 1981], pointing to the possibility of scattering losses. However, in analyzing the possible wave-particle interactions of electrons in the torus, Thorne and Tsurutani [1979] found that the maximum precipation flux allowed by pitch angle scattering amounts to about 10^{13} W, well below the range required to account for the X ray flux by electron bremsstrahlung. Furthermore, most of this energy stems from incident electrons in the energy range of 0.15-3 MeV, for which atmospheric extinction of UV emission would become a major correction and for which the X ray spectrum would be harder than observed. Other scattering modes resonating with 10 keV and less deposit less energy into the atmosphere [Thorne, 1982]. On the basis of Pioneer data, Thomsen and Sentman [1979] have calculated even lower energy deposition rates for electrons undergoing pitch angle scattering into the atmosphere. We conclude that electron bremsstrahlung is not the source of the X ray emission and most likely not of the UV emission either.

4.4. Heavy Ion Precipitation

The inability of electron precipitation to supply sufficient energy for the aurora and the accompanying requirement for a mass loading rate in excess of the value inferred from observation of the torus has led Thorne [1981, 1982] and Gehrels and Stone [1983] to propose that ions of S and O, which dominate the ion component in the Io torus [Bagenal and Sullivan, 1981], also comprise the precipitating flux at Jupiter. Evidence for this lies in the existence of an inward radial gradient for the energized heavy ion flux, indicating injection from the outer magnetosphere [Gehrels et al., 1981], and the contrast between a constant flux measured between 12 and 17 R_J and a sharp decrease between 6 and 12 R_J [Gehrels and Stone, 1982]. This indicates a rapid precipitation loss of these heavy ion fluxes at a rate comparable to the limit imposed by strong pitch angle diffusion.

The scheme envisaged by Gehrels and Stone [1983] is that Iogenic S and O plasma ions diffuse outward from the torus, undergo nonadiabatic acceleration by a process as yet not established and subsequently diffuse inward as an energetic flux distribution, a large fraction of which undergoes scattering into the loss cone and precipitation into Jupiter's atmosphere. The energy associated with these particles results in highly-stripped ionization states, and the subsequent slowing down in the atmosphere invariably results in radiative transitions. From the observed loss rate of S and O ions, Gehrels and Stone [1983] have calculated the power and flux delivered to Jupiter as a function of ion energy. We have used their distributions to calculate the expected yield of X rays that would be produced by the interaction of these heavy ions with the hydrogen atmosphere. The X ray flux will be confined to 0.52 keV (O) and 2.3 keV (S) if O and S alone

comprise the incident flux. Secondary electrons will be low in both energy and yield.

The cross-sections used for this calculation were obtained from data for line production by proton bombardment given by Garcia et al. [1973] with the appropriate correction for this case of heavy ions incident on hydrogen. The cross-sections become appreciable above energies of about 10 keV/nucleon. The Voyager cosmic ray experiment energy threshold of 6 MeV/nucleon was extrapolated down to an energy of 0.6 MeV/nucleon by Gehrels and Stone [1983] through the use of data obtained with the LECP instrument [Armstrong et al., 1981], and we have extrapolated below that to a cumulative power level of $\sim 10^{14}$ W in order to extend the calculation down to the energy at which characteristic X ray production is no longer significant ($\sim$0.1 MeV/nucleon). The penetration of incident O and S ions in the hydrogen atmosphere was determined from a range-energy table [Northcliffe and Schilling, 1970]. This range is small in comparison with that of the observed X rays so that extinction losses are negligible. We find that the calculated X ray power from O ions amounts to about 4×10^9 W and that from S ions amounts to about 10^8 W. Comparison with our observed values in Table 5 shows excellent agreement for the oxygen-induced emission. The calculated values will change somewhat when the effect of ion charge state is incorporated in the analysis, but the general correspondence, particularly in the relative proportions of O and S line fluxes, is clear indication that heavy ion precipitation is responsible for Jupiter's X ray aurora.

Taking into consideration the abundance of energetic protons just beyond the torus [Krimigis et al., 1979], the composition of Jupiter's upper atmosphere [Atreya et al., 1981] and the appropriate cross-sections for line emission [Garcia et al., 1973], proton precipitation fails to account for the observed X ray flux by a factor exceeding 10^3.

The X ray observations to date show little if any variation with time. This contrasts with observations in the UV where substantial long and short term variability has been observed [Broadfoot et al., 1981; Durrance et al., 1982]. While the weak signal of these initial X ray observations makes variation harder to observe, there does appear to be a real distinction, indicating the mechanism of production at the two wavelengths may not be identical. An opportunity of a closer look at this exists for the 1981 HRI observation during which Jupiter was observed simultaneously by the Einstein Observatory and the International Ultraviolet Explorer.

In summary, X ray emission from 0.2-3.0 keV has been detected from the auroral zones of Jupiter. The spectrum is soft, the total flux relatively constant. Attempts to attribute the source of the X ray flux to electron bremsstrahlung fail on the combined argument of the total power and energy spectrum. On the other hand, the expected yield from energetic O and S ions precipitating into the atmosphere is in good agreement with observations.

An EXOSAT observation of Jupiter is currently scheduled which should yield more information on the low-energy X ray spectrum and time variations. Future observations with increasingly sensitive X ray observatories allow us to anticipate the possibility of positive results from Saturn, Uranus, and Neptune as well. Observations of the Jovian system with such instruments will yield more detail, notably on the interaction of energetic particles with the Galilean satellites and Jupiter's rings. Someday it should be possible to determine their surface compositions in this manner.

Acknowledgments. The research described in this paper was carried out in part by the Jet Propulsion Laboratory, California Institute of Technology, under contract with the National Aeronautics and Space Administration. We acknowledge with appreciation the assistance of Dan Harris and Robert Radocinski in providing computer support for the data analysis and that of F. R. Harnden, Jr., for advice and assistance in applying the FINSPEC spectral fitting routine to the IPC data. We thank Paul Joss, George Siscoe, and J. D. Garcia for helpful discussions, and Bruce Tsurutani for a thorough and constructive review of the manuscript.

The Editor thanks E. Kirsch and C. K. Goertz for their assistance in evaluating this paper.

References

Adler, I., J. Trombka, J. Gerard, R. Schmadebeck, P. Lowman, H. Blodgett, L. Yin, E. Eller, R. Lamothe, P. Gorenstein, P. Bjorkholm, B. Harris, and H. Gursky, X-Ray fluorescence experiment, Apollo 15 Preliminary Science Report, NASA SP-289, 1972.

Armstrong, T. P., M. C. Paonessa, S. T. Brandon, S. M. Krimigis, and L. J. Lanzerotti, Low energy charged particle observations in the 5-20 R_J region of the Jovian magnetosphere, J. Geophys. Res., 86, 8343, 1981.

Atreya, S. K., T. M. Donahue, and M. C. Festou, Jupiter: Structure and composition of the upper atmosphere, Astrophys. J., 247, L43, 1981.

Bagenal, F., and J. D. Sullivan, Direct plasma measurements in the Io torus and inner magnetosphere of Jupiter, J. Geophys. Res., 86, 8447, 1981.

Berge, G. L., and S. Gulkis, Earth-based radio observations of Jupiter: Millimeter to meter wavelengths in Jupiter, edited by T. Gehrels, p. 621, University of Arizona Press, Tucson, 1976.

Borovsky, J. E., C. K. Goertz, and G. Joyce, Magnetic pumping of particles in the outer Jovian magnetosphere, J. Geophys. Res., 86, 3481, 1981.

Bridge, H. S., J. W. Belcher, A. J. Lazarus, J. D. Sullivan, R. J. McNutt, F. Bagenal, J. E. Scudder, E. Z. Sittler, J. L. Siscoe, D. M. Vasyliunas, C. K. Goertz, and C. M. Yeates, Plasma observations near Jupiter: Initial results from Voyager 1, Science, 204, 987, 1979.

Broadfoot, A. L., M. J. S. Belton, P. Z. Takacs, D. E. Sandel, J. B. Shemansky, J. M. Holberg, S. K. Ajello, T. M. Atreya, H. W. Donahue, J. L. Moos, J. E. Bertaux, D. F. Blamont, J. C. Strobel, A. McConnell, F. Dalgarno, F. Goody,

and M. B. McElroy, Extreme ultraviolet observations from Voyager 1 encounter with Jupiter, Science, 204, 979, 1979.

Broadfoot, A. L., B. R. Sandel, D. E. Shemansky, J. D. McConnell, G. R. Smith, J. D. Holberg, S. K. Atreya, T. M. Donahue, D. F. Strobel, and J. L. Bertaux, Overview of the Voyager ultraviolet spectrometry results through Jupiter encounter, J. Geophys. Res., 86, 8259, 1981.

Brown R. A., The Jupiter hot plasma torus: Observed electron temperature and energy flow, Astrophys. J., 244, 1072, 1981.

Cheng, A. F., Effects of Io's Volcanos on the plasma torus and Jupiter's magnetosphere, Astrophys. J., 242, 812, 1980.

Coroniti, F. V., F. L. Scarf, C. F. Kennel, W. S. Kurth, and D. A. Gurnett, Detection of Jovian whistler mode chorus: Implications for the Io torus aurora, Geophys. Res. Lett., 7, 45, 1980.

Dessler, A. J., Mass-injection rate from Io into the Io plasma torus, Icarus, 44, 291, 1980.

Durrance, S. T., P. D. Feldman, and H. W. Moos, The spectrum of the jovian aurora 1150-1700 A, Geophys. Res. Lett., 9, 652, 1982.

Edwards, P. J. and K. G. McCracken, Upper limits to the hard X ray flux from the quiet sun and Jupiter, J. Geophys. Res., 72, 1809, 1967.

Eviatar, A., and G. L. Siscoe, Limit on rotational energy available to excite Jovian aurora, Geophys. Res. Lett., 7, 1083, 1980.

Fisher, P. C., D. B. Clark, A. J. Meyerott, and K. L. Smith, Upper limit to Jupiter's X-ray flux on September 30, 1972, Nature, 204, 982, 1964.

Garcia, J. D., R. J. Fortner, and T. M. Kavanagh, Inner-shell vacancy production in ion-atom collisions, Rev. Mod. Phys., 45, 111, 1973.

Gehrels, N., and E. C. Stone, Energetic oxygen and sulfur in the Jovian magnetosphere and their contribution to the auroral excitation, J. Geophys. Res., 88, 5537, 1983.

Gehrels, N., E. C. Stone, and J. H. Trainor, Energetic oxygen and sulfur in the jovian magnetosphere, J. Geophys. Res., 86, 8906, 1981.

Giacconi, R., G. Branduardi, U. Briel, A. Epstein, D. Fabricant, E. Feigelson, W. Forman, P. Gorenstein, J. Grindlay, H. Gursky, F. R. Harnden, Jr., J. P. Henry, C. Jones, E. Kellogg, D. Koch, S. Murray, E. Schreier, F. Seward, H. Tananbaum, K. Topka, L. Van Speybroeck, S. S. Holt, R. H. Becher, E. A. Boldt, P. J. Serlemitsos, G. Clark, C. Canizares, T. Markert, R. Novick, D. Helfand, and K. Long, The Einstein (HEAO-2) X-ray observatory, Astrophys. J., 230, 540, 1979.

Giles, J. W., H. W. Moos, and W. R. McKinney, The far ultraviolet (1200-1900A) spectrum of Jupiter obtained wth a rocket-borne multichannel spectrometer, J. Geophys. Res., 81, 5797, 1976.

Goertz, C. K., Io's interaction with the plasma torus, J. Geophys. Res., 85, 2949, 1980a.

Goertz, C. K., Proton aurora on Jupiter's nightside, Geophys. Res. Lett., 7, 365, 1980b.

Gorenstein, P., F. R. Harnden, Jr., and D. G. Fabricant, In orbit performance of the Einstein Observatory/HEAO-2 Imaging Proportional Counter, IEEE Trans. Nucl. Sci., NS-283, 869, 1981.

Haymes, R. C., D. V. Ellis, and G. J. Fishman, Upper limits to the hard X ray fluxes from Mars, Venus, and Jupiter, J. Geophys. Res., 73, 867, 1968.

Heaps, M. G., J. N. Bass, and A. E. S. Green, Electron excitation of a Jovian aurora, Icarus, 20, 297, 1973.

Hill, T. W., Inertial limit on corotation, J. Geophys. Res., 84, 6554, 1979.

Hurley, K. C., Search for X-rays from the planet Jupiter, J. Geophys. Res., 77, 46, 1972.

Hurley, K. C., Upper limits to jovian X-ray emission from the UHURU satellite, in The Magnetospheres of the Earth and Jupiter, edited by V. Formisano, p. 241, D. Reidel, Hingham, Mass., 1975.

Jones A. V., Aurora, D. Reidel, Hingham, Mass., 1974.

Kirsch, E., S. M. Krimigis, J. W. Kohl, and E. P. Keath, Upper limits for X ray and energetic neutral particle emission from Jupiter: Voyager 1 results, Geophys. Res. Lett., 8, 169, 1981.

Krimigis, S. M., T. P. Armstrong, W. I. Axford, C. O. Bostrom, C. Y. Fan, G. Gloeckler, L. J. Lanzerotti, E. P. Keath, R. D. Zwickl, J. F. Carbary, and D. C. Hamilton, Hot plasma environment at Jupiter: Voyager 2 results, Science, 206, 977, 1979.

Lanzerotti, L. J., C. G. Maclennan, T. P. Armstrong, S. M. Krimigis, R. P. Lepping, and N. F. Ness, Ion and electron angular distributions in the Io torus region of the Jovian magnetosphere, J. Geophys. Res., 86, 8491, 1981.

Mahoney, W. A., Hard X-ray spectra of discrete cosmic sources, Ph.D. thesis, Univ. of Calif. Berkeley, 1973.

Metzger, A. E., D. A. Gilman, J. L. Luthey, K. C. Hurley, J. D. Sullivan, F. D. Seward, and H. W. Schnopper, Observation of X-rays from the Jovian system, Bull. Am. Astron. Soc., 12 (#2), 450, 1980.

Metzger, A. E., D. A. Gilman, J. L. Luthey, K. C. Hurley, H. W. Schnopper, F. D. Seward, and J. D. Sullivan, The detection of X-rays from Jupiter, Eos Trans. AGU, 62, 374, 1981.

Mihalov, J. D., On limits to Jupiter's magnetospheric diffusion rates, Astrophys. Space Sci., 20, 483, 1973.

Mizera, P. F., J. G. Luhmann, W. A. Kolasinski, and J. B. Blake, Correlated observations of auroral arcs, electrons and X-rays from a DMSP satellite, J. Geophys. Res., 83, 5573, 1978.

Northcliffe, L. C., and R. F. Schilling, Range and stopping-power tables for heavy ions, Nucl. Data Tables, A7, 233, 1970.

Opp, A. G., Pioneer 10 mission: Summary of scientific results from the encounter with Jupiter, Science, 188, 302, 1974.

Opp, A. G., Scientific results from the Pioneer 11 Mission to Jupiter, Science, 188, 447, 1975.

Pages, L., E. Bertel, H. Joffre, and L. Skavenitis, Energy-loss range and bremsstrahlung yield for 10-keV to 100-MeV electrons in various elements and chemical compounds, At. Data, 4, 1, 1972.

Peale, S. J., P. Cassen, and R. T. Reynolds, Melting of Io by tidal dissipation, Science, 203, 892, 1979.

Pratt, R. H., H. K. Tseng, C. M. Lee, L. Kissel,

C. MacCallum, and M. Riley, Bremsstrahlung energy spectra from electrons of kinetic energy 1 keV <=T_1<=2000 keV incident on neutral atoms 2<=Z<=92, At. Data and Nucl. Data Tables, 20, 175, 1977.

Rugge, H. R., D. L. McKenzie, and P. A. Charles, HEAO-1 Observation of X-ray fluorescence emission lines from the earth's sunlit atmosphere, in Space Research, p. 243, Pergamon, New York, 1978.

Sandel, B. R., D. E. Shemansky, A. L. Broadfoot, J. L. Bertaux, J. E. Blamont, J. J. S. Belton, J. M. Ajello, J. B. Holberg, S. K. Atreya, T. M. Donahue, H. W. Moos, D. R. Strobel, J. C. McConnell, A. Dalgarno, R. Goody, M. B. McElroy, and P. Z. Takacs, Extreme ultraviolet observations from Voyager 2 encounters with Jupiter, Science, 206, 962, 1979.

Seltzer, S. M. and M. J. Berger, Bremsstrahlung in the atmosphere at satellite altitudes, J. Atmos. Terr. Phys., 36, 1283, 1974.

Shemansky, D. E., Mass loading and the diffusion loss rates of the Io plasma torus, Astrophys. J., 242, 1266, 1980.

Shemansky, D. E., and B. R. Sandel, Injection of energy into the Io plasma torus, J. Geophys. Res., 87, 219, 1982.

Stone, E. C., The Voyager mission through the Jupiter encounters, J. Geophys. Res., 86, 8123, 1981.

Thomsen, N. F., and T. D. Sentman, Precipitation fluxes of energetic electrons at Jupiter: An estimated upper limit, J. Geophys. Res., 84, 1409, 1979.

Thorne, R. M., Jovian auroral secondary electrons and their influence on the Io plasma torus, Geophys. Res. Lett., 8, 509, 1981.

Thorne, R. M., Microscopic plasma processes in the jovian magnetosphere, in Physics of the Jovian Magnetosphere, edited by A. J. Dessler, p. 454, Cambridge University Press, New York, 1982.

Thorne, R. M., and B. T. Tsurutani, Diffuse jovian aurora influenced by plasma injection from Io, Geophys. Res. Lett., 6, 649, 1979.

Veigele, W. J., Photon cross sections from 0.1 keV to 1 MeV for elements Z = 1 to Z = 94, At. Data Tables, 5, 51, 1973.

Vesecky, J. F., J. R. Culhane, and F. J. Hawkins, Upper limits for X-ray emission from Jupiter as measured from the Copernicus satellite, in The Magnetospheres of the Earth and Jupiter, p. 245, edited by V. Formisano, ed., D. Reidel, Hingham, Mass., 1975.

Yung, Y. L., G. R. Gladstone, K. M. Chang, J. M. Ajello, and S. K. Srivastava, H_2 fluorescence spectrum from 1200 to 1700A by electron impact: Laboratory study and application to jovian aurora, Astrophys. J., 254, L65, 1982.

Winters, L., M. D. Brown, L. D. Ellsworth, J. Chiao, E. W. Pettus, and J. R. Macdonald, K X-ray production in single collisons of chlorine and sulfur ions, Phys. Rev. A., 11, 174, 1975.

J. L. Luthey, and A. E. Metzger, Jet Propulsion Laboratory, California Institute of Technology, Pasadena, CA 91109.

D. A. Gilman, National Aeronautics and Space Administration, Washington, DC 20546.

K. C. Hurley, Centre d'Etude Spatiale des Rayonnements, CNRS-UPS, BP 4346, 31029 Toulouse, France

H. W. Schnopper, Danish Space Research Institute, Lundtostvej 7, DK-2800, Lyngby, Denmark.

F. D. Seward, Smithsonian Astrophysical Observatory, Cambridge, MA 02139.

J. D. Sullivan, Plasma Fusion Center, Massachusetts Institute of Technology, Cambridge, MA 02139.

(Received March 14, 1983;
revised June 17, 1983;
accepted June 20, 1983.)

DUMP OF TAPE KM2004

D73981

78-103A-02C / HEAD 2

INPUT TAPE KM2004 ON HT1
DATA INPUT F9 NF 1 FL 1 3 3

FILE 1 RECORD 1 LENGTH 2880BYTES

(0)	53494D5[illegible]	4C452020	3D202020	20202020	20202020	20202020	20202020	20542020	20202020	20202020
(40)	2F20434F	4E464F52	4D532054	4F204241	53494320	464F524D	41543F20	20202020	20202020	20202020
(80)	42495453	49582020	3D202020	20202020	20202020	20202020	20202020	31362020	20202020	20202020
(120)	2F2[illegible]4249	54532[illegible]5	45522[illegible]5	4958454C	20202020	20202020	20202020	20202020	20202020	20202020
(160)	4E415849	53202020	3D2[illegible]2020	20202020	20202020	20202020	20202020	20322020	20202020	20202020
(200)	2F2 4E55	4D424552	204F4620	41584953	20202020	20202020	20202020	20202020	20202020	20202020
(240)	4E415849	53312020	3D20[illegible]020	20202020	20202020	20202020	20202032	35362020	20202020	20202020
(280)	2F2[illegible]5241	20202020	20415849	53204449	4D454E53	494F4E20	20202020	20202020	20202020	20202020
(320)	4E415849	53322020	3D202020	20202020	20202020	20202020	20202032	35362020	20202020	20202020
(360)	2F2[illegible]4445	43202020	20415849	53204449	4D454E53	494F4E20	20202020	20202020	20202020	20202020
(400)	2[illegible]2[illegible]2[illegible]	20202020	20[illegible]2020	20202020	20202020	20202020	20202020	20202020	20202020	20202020
(440)	2[illegible]2[illegible]2020	20202020	20[illegible]2020	20202020	20202020	20202020	20202020	20202020	20202020	20202020
(480)	42534341	4C452020	3D202020	20202020	20202020	20202E30	30303530	30302020	20202020	20202020
(520)	2F2[illegible]5452	55452030	20585441	50452A42	53434140	45502B42	5A45524F	20202020	20202020	20202020
(560)	425A4552	4F202020	3D2[illegible]020	20202020	20202020	20202020	20202020	20302020	20202020	20202020
(600)	2F204F46	46534554	20544F20	54525545	20594958	454C2056	414C5545	53202020	20202020	20202020
(640)	44415441	4D415820	3D202020	20202020	20202020	20202020	20203430	30302020	20202020	20202020
(680)	2F2[illegible]4D41	58205641	4C554520	4F462041	52524159	20202020	20202020	20202020	20202020	20202020
(720)	2[illegible]2[illegible]2020	20202020	20[illegible]2020	20202020	20202020	20202020	20202020	20202020	20202020	20202020
(760)	2[illegible]2020	20202020	20[illegible]2020	20202020	20202020	20202020	20202020	20202020	20202020	20202020
(800)	43525641	4C312020	3D202020	20202020	20202031	38392E31	38373830	30302020	20202020	20202020
(840)	2F2[illegible]5241	20[illegible]2020	20524546	20504F49	4E542056	414C5545	20284445	47292020	20202020	20202020
(880)	43525049	58312020	3D2[illegible]020	20202020	20202020	37372E30	30303030	30302020	20202020	20202020
(920)	2F2[illegible]5241	20202020	20524546	20504F49	4E542050	4958454C	204C4F43	4154494F	4E202020	20202020
(960)	4344454C	54312020	3D2[illegible]020	20202020	20202020	202D2E30	30303237	37382020	20202020	20202020
(1000)	2F2[illegible]5241	20[illegible]2020	20494E43	52454D45	4E542041	4C4F4E47	20415849	53202844	45472920	20202020
(1040)	43545950	45312020	3D202[illegible]4C	4C202020	20202027	20202020	20202020	20202020	20202020	20202020
(1080)	2F2[illegible]5241	20202020	20545950	45202020	20202020	20202020	20202020	20202020	20202020	20202020
(1120)	43524F54	41312020	3D2[illegible]020	20202020	20202020	20202E30	30303030	30302020	20202020	20202020
(1160)	2F2[illegible]5241	20202020	20524F54	4154494F	4E202020	20202020	20202020	20202020	20202020	20202020
(1200)	43525641	4C322020	3D202020	20202020	20202020	20322E35	31333035	33302020	20202020	20202020
(1240)	2F2[illegible]4445	43202020	20524546	20504F49	4E542056	414C5545	20284445	47292020	20202020	20202020
(1280)	43525049	58322020	3D2[illegible]020	20202020	20202031	34322E30	30303030	30302020	20202020	20202020
(1320)	2F2[illegible]4445	43202020	20524546	20504F49	4E542050	4958454C	204C4F43	4154494F	4E202020	20202020
(1360)	4344454C	54322020	3D202020	20202020	20202020	202D2E30	30303237	37382020	20202020	20202020
(1400)	2F2[illegible]4445	43202020	20494E43	52454D45	4E542041	4C4F4E47	20415849	53202844	45472920	20202020
(1440)	4354595[illegible]	45322020	3D2[illegible]274C	4D202020	20202027	20202020	20202020	20202020	20202020	20202020
(1480)	2F2[illegible]4445	43202020	20545950	45202020	20202020	20202020	20202020	20202020	20202020	20202020
(1520)	43524F54	41322020	3D202020	20202020	20202020	20202E30	30303030	30302020	20202020	20202020
(1560)	2F2[illegible]4445	43202020	20524F54	4154494F	4E202020	20202020	20202020	20202020	20202020	20202020
(1600)	2[illegible]2[illegible]2020	20202020	20[illegible]2020	20202020	20202020	20202020	20202020	20202020	20202020	20202020
(1640)	20202020	20202020	20202020	20202020	20202020	20202020	20202020	20202020	20202020	20202020
(1680)	41525220	54595045	3D2[illegible]020	20202020	20202020	20202020	20342020	20202020	20202020	20202020
(1720)	2F2[illegible]313D	44502C33	3D465[illegible]2C	3430492C	2D39333D	4E4F4E2D	41525241	59202020	20202020	20202020
(1760)	524F4C4C	2D414E47	3D2[illegible]020	20202020	20202020	202D2E30	30303030	30302020	20202020	20202020
(1800)	2F2[illegible]4249	4E4E4544	20524F4C	4C20414E	474C4520	20202020	20202020	20202020	20202020	20202020
(1840)	54494C45	2D4F4253	3D2[illegible]020	20202020	20323037	32352E37	36303030	30302020	20202020	20202020
(1880)	2F2[illegible]4F42	53455256	4154494F	4E205449	4D452E53	45432920	20202020	20202020	20202020	20202020
(1920)	54494D45	2D494D47	3D202020	20202020	20203835	37322E34	37333030	30302020	20202020	20202020
(1960)	2F2[illegible]5449	4D452049	4E2[illegible]152	4F434553	53454420	494D4147	45202020	20202020	20202020	20202020
(2000)	5345514E	4F2[illegible]20	3D2[illegible]020	20202020	20202020	2[illegible]202020	20302020	20202020	20202020	20202020
(2040)	2F2[illegible]5345	5155454E	43452[illegible]4E	554D4245	52202020	20202020	20202020	20202020	20202020	20202020
(2080)	494[illegible]5354	52554D45	3D202748	52492020	20202027	20202020	20202020	20202020	20202020	20202020
(2120)	2F2[illegible]4549	4E535445	494E2049	4E535452	554D454E	54202020	20202020	20202020	20202020	20202020
(2160)	4F42[illegible]45	52564552	3D2[illegible]743	46412[illegible]	2[illegible]202027	2[illegible]202020	20202020	20202020	20202020	20202020
(2200)	2F2 4F42	53455256	45522753	204E4140	452[illegible]20	2[illegible]202020	2[illegible]202020	2[illegible]202020	2[illegible]202020	20202020
(2241)	42554E49	54202020	3D202743	54532F3F	20202027	20202020	20202020	20202020	20202020	20202020
(2281)	2F2 4252	49474854	4E[illegible]5353	20554E49	542[illegible]20	2[illegible]202020	20202020	20202021	20202020	20202020